ADVANCED MATERIALS
www.advmat.de

Artificial Tendrils Mimicking Plant Movements by Mismatching Modulus and Strain in Core and Shell

Muhammad Farhan, Frederike Klimm, Marc Thielen, Andraž Rešetič, Anil Bastola, Marc Behl, Thomas Speck,* and Andreas Lendlein**

Motile organs have evolved in climbing plants enabling them to find a support and, after secure attachment, to reach for sunlight without investing in a self-supporting stem. Searching movements, the twining of stems, and the coiling of tendrils are involved in successful plant attachment. Such coiling movements have great potential in robotic applications, especially if they are reversible. Here, the underlying mechanism of tendril movement based on contractile fibers is reported, as illustrated by a function–morphological analysis of tendrils in several liana species and the encoding of such a principle in a core–shell multimaterial fiber (MMF) system. MMFs are composed of a shape-memory core fiber (SMCF) and an elastic shell. The shape-memory effect of the core fibers enables the implementation of strain mismatch in the MMF by physical means and provides thermally controlled reversible motion. The produced MMFs show coiling and/or uncoiling behavior, with a high reversible actuation magnitude of ≈400%, which is almost 20 times higher compared with similar stimuli for sensitive soft actuators. The movements in these MMFs rely on the crystallization/melting behavior of oriented macromolecules of SMCF.

1. Introduction

The diversified motility patterns and underlying structures found in plants are a result of evolution, namely the long-term interplay between mutation, recombination, and selection that lead to a plant's adaptation to its local environments. The various motions in plants range from the snapping of Venus flytraps to the opening of seedpods and the bending of wheat awns to the coiling of tendrils in climbing plants.[1] As opposed to trees, which possess a solid massive self-supporting stem, climbing plants mainly rely on external supporting structures to hoist themselves upward.[2] Many climbers such as the passionflowers *Passiflora caerulea* or *Passiflora discophora* (see **Figure 1**A) attach to these supports by using filamentary organs sensitive to contact (tendrils) with or without adhesive pads.[2b] A typical tendril performs three different types of subsequent movement: 1) a "searching" movement whereby the free tendril circulates (autonomous circumnutation), 2) an "attaching" movement during which the tendril's tip either develops adhesive pads or coils around a support upon making contact (contact coiling), and 3) a "coiling" movement of the tendril axis resulting in its characteristic spring-like appearance pulling the stem of the liana closer to the support (free coiling).[2b,3] An inequality of length between the two sides of a tendril has long been recognized as a cause for the free coiling movement.[3c] The length and therefore strain

M. Farhan, A. Rešetič[+], A. Bastola[++], M. Behl, A. Lendlein
Institute of Active Polymers
Helmholtz-Zentrum Hereon
Kantstr. 55, 14513 Teltow, Germany
E-mail: Muhammad.Farhan@hereon.de; andreas.lendlein@gmail.com

The ORCID identification number(s) for the author(s) of this article can be found under https://doi.org/10.1002/adma.202211902

[+]Present address: Jožef Stefan Institute, Solid State Physics Department, Jamova cesta 39, 1000 Ljubljana, Slovenia

[++]Present address: Centre for Additive Manufacturing (CfAM), School of Engineering, University of Nottingham, Nottingham NG8 1BB, UK

DOI: 10.1002/adma.202211902

F. Klimm, M. Thielen, T. Speck
Plant Biomechanics Group
Institute of Biology
University of Freiburg
79104 Freiburg, Germany
E-mail: thomas.speck@biologie.uni-freiburg.de

F. Klimm, T. Speck
Cluster of Excellence *liv*MatS @ FIT-Freiburg Center for Interactive Materials and Bioinspired Technologies
University of Freiburg
Georges-Köhler-Allee 105, 79110 Freiburg, Germany

F. Klimm, M. Thielen, T. Speck
FMF – Freiburg Materials Research Center
Stefan-Meier-Straße 21, 79104 Freiburg, Germany

A. Lendlein
Institute of Chemistry
University of Potsdam
14469 Potsdam, Germany

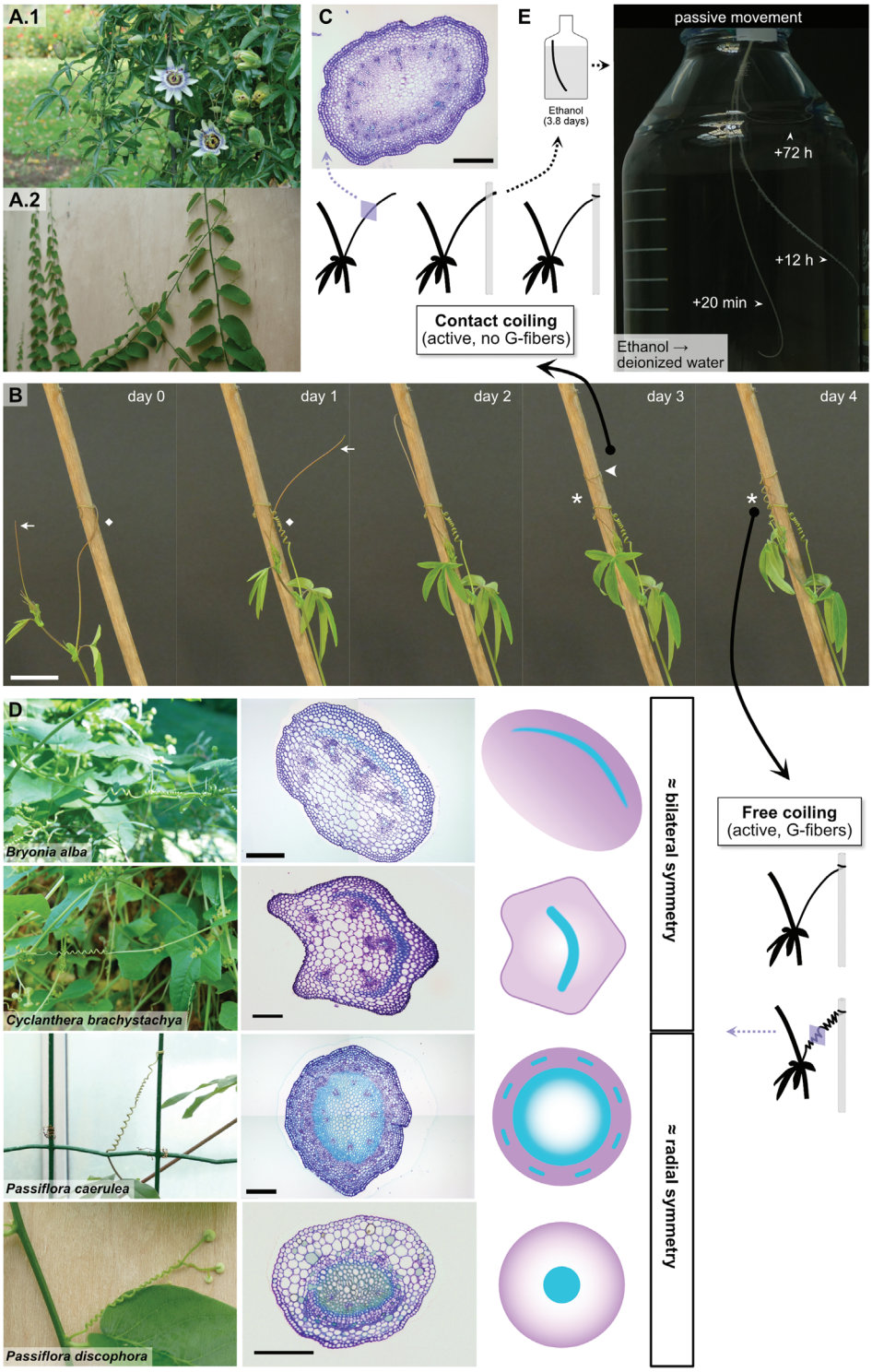

Figure 1. Tendril-bearing climbing plants and tendril movements: Passion flowers climbing on a trellis (*P. caerulea*, A.1) or a flat wooden board (*P. discophora*, A.2). Both attach themselves to their supports by means of tendrils. During its development, a tendril of *P. caerulea* first circumnutates (arrow) and touches a support whereupon it fastens via contact coiling (arrowheads). B) Then, once its tip is fixed, the tendril starts coiling along its own axis (asterisk), which can also be observed for the older tendril that had previously attached itself to the pole (diamond). C) Toluidine-blue stained cross sections show the anatomy of a yet unattached tendril of *P. caerulea*, sensitive to coil upon contact, D) and of tendrils that have performed free coiling (various climbing plant species). Schematic drawings highlight the tissue arrangement and the mechanical tissues (G-fibers and/or lignified tissues colored green-blue) and suggest a grouping into bilateral symmetric and radial symmetric tendrils. In addition to the active contact and free coiling, an excised and fixated tendril also curves passively, when transferred from the fixative (ethanol) to deionized water (transparent superimposition of video stills 20 min, 12, and 72 h after media change) (E). Scale bars: 200 µm (C,D) and 2 cm (B).

mismatch between the two sides leads to an intrinsic curvature of the tendril that drives the coiling process.[4] It results in the formation of a "twistless spring".[4] Since both ends of the tendril are fixed, the tendril obtains a shape with a minimum of two helices of opposite handedness with identical numbers of left- and right-handed windings, connected by a so-called perversion as shown in Figure 1B.[2b,3c,4,5] Several biological processes have been proposed to be involved in the free and contact coiling movements of tendrils, such as differential growth, that is, one side of the tendril grows relatively faster than the other side,[3a,b] osmotic effects causing certain cells of the tendril to swell/shrink because of water absorption/desorption,[3a,b,6] or the development of contractile fibers[7] that are possibly fine-tuned via variations in lignification and microfibril orientation.[8]

The formation of an elastic spring-like shape during the free coiling movement in climbing plants serves both to draw the stem closer to its substrate and to form a dampening structure to prevent critical damage to the plant during wind gusts or other external mechanical loading events.[2b,3c,9] Such resilient fixation strategies and attachment modes are however also important features for soft robots designed to move by growing and to navigate through unknown terrain.[10] Therefore, an understanding and the technical replication of tendril-like movements are of great importance for applications in soft robotic technology for which adaptive movements are required. Hence, the coiling of plant structures has been intensively studied.[11]

Special attention has been given to biomimetic innovations in robotics. On the one hand, the incorporation of specific built-in strain mismatch in artificial materials has produced plant-like coiling,[12] whereas on the other hand, self-shaping materials have been designed with tunable internal stress in response to external stimuli.[13] A promising approach for mimicking plant-like movements are multifunctional multimaterial systems in which an orchestrated interplay of functions can provide the desired coiling behavior. These multimaterial systems include composite materials having dissimilar properties in different layers. A 3D-printing approach has been used to develop a polymer–paper bilayer composite[14] that coils upon heating as a result of strain recovery of the polymer layer. The strain is stored via the stretching of the melted polymer filament during the printing process, with the paper layer acting as a passive strain-limiting layer. In an extension to this, dual responsive bilayers have been created that coil in response to both heat and water by the incorporation of a water-responsive hydrophilic polymer as the first layer and a heat-responsive liquid crystal elastomer as the second layer.[15] In addition to these approaches, single-layer hydrogel sheets with chemically distinct small-scale fiber-like patterns have been reported that exhibit differential shrinkage and elastic moduli under the application of an external stimulus to give cylindrical and conical helices with specific structural characteristics.[16] These approaches mainly rely on complex synthesis strategies and are often limited by achieving only one coil, and lack reversible movements.

In this study, we illustrate and discuss coiling principles in plant tendrils from *Bryonia alba*, *Cyclanthera brachystachya*, *P. caerulea*, and *P. discophora* based on macroscopic observations and light microscopic analyses of cross sections of their tendrils. Inspired by tendril anatomy and the mechanisms of translating of phase behavior to macroscopic motion, we have designed multimaterial fibers (MMFs) with a tough shape-memory core fiber (SMCF) and an elastically deformable matrix. The shape-memory effect is used to implement core–shell strain differences by physical means during MMF fabrication or in a post fabrication step. Programing of SMCF by stretching respectively the contraction of SMCF upon heat mimics the differentiation processes observed in biological role models during coiling due to the shortening caused by the development of (lignified) G-fibers or coiling due to shrinkage (attributable to water loss). In our technical MMF system, we even go beyond nature by exploring the full functional spectrum of SMCF including twist-programing or thermally controlled reversible actuation.

2. Results and Discussion

The anatomical organization (i.e., the material composition) of climbing plant tendrils differs between the two coiling motions that the tendrils perform during their ontogeny (Figure 1). Young, unattached tendrils of, for example, *P. caerulea* are almost entirely composed of parenchymatous (soft) tissues (Figure 1C), and when they come in contact with an object, they coil rapidly, most likely due to osmotic effects and differential growth.[6] In contrast to that, tendrils that are attached and have coiled along their length (free coiling), show a distinct band or core region of stiff cells embedded in the parenchymatous tissues (Figure 1D, various plant species). These probably represent G-fibers, which are specialized cells with contractile properties (details can be found in Supporting Information). In tendrils of the exploding cucumber (*C. brachystachya*) and white bryony (*B. alba*), the G-fiber band is positioned on one side of the tendril, that is, the tendrils have a bilateral symmetric tissue organization. This suggests a straightforward way for inducing coiling by a contractile region positioned on the "inside-to-be" (later concave side) of the tendril. However, tendrils from other species, such as the passion flowers *P. discophora* and *P. caerulea*, do not show an obvious bilateral symmetric tissue arrangement. Rather, in the fully coiled state, they have G-fibers positioned in a distinct core region being circular or elliptical in cross section (Figure 1D). However, it has been shown that during the coiling movement, tissue development (i.e., the formation of lignified tissue) on the concave side precedes that on the convex side in *P. caerulea* tendrils, indicating that the G-fibers first form only on the concave side.[17] Therefore, we expect the coiling movement to function by a similar principle as in case of an eccentric arrangement of contractile tissues outlined above. Except that here, this arrangement represents only a specific stage in the development, that is, is only found at a specific time period during ontogeny, before the formation of woody tissue with G-fibers is completed across the entire center of the cross section. Similar coiling principles can thus be expected for the four species, namely a strain mismatch resulting from either a non-radial symmetric arrangement of contractile tissues or the spatially non-uniform ontogenetic development of contractile tissues.

Based on these results, we have developed artificial tendrils from a soft shell material (with a low modulus $E = 1.8 \pm 0.4$ MPa) and a stiffer core material (with a high $E = 30 \pm 2$ MPa) that contracts relative to the shell combined with an eccentrically positioned core. Further, in tendrils of cucumber and wild cucumber (*Cucumis sativus* and *Echinocystis lobata*), a ribbon–like fiber

layer has been suggested to work alone as the actuator for the shape change that occurs during coiling, whereas the surrounding soft tissue passively follows this movement.[8] Asymmetric contraction of the two-layered fiber ribbon itself should lead to coiling, as illustrated by a physical model made from two differentially pre-strained silicon rubber layers bonded together.[8] In contrast, our present study focuses on developing multimaterial fibers from materials with a dissimilar *E*-modulus ratio of core and shell at various temperatures. Accordingly, our artificial tendrils can be equipped with additional layers, if required, that will be passively moved by the actuating shell/core construction. Here, a more precise fiber-processing method such as the thermal drawing technique can be used to fabricate multilayer multimaterial fibers with complex architectures at the micro- and nanoscales with ensured reproducibility and precision.[18]

Both free coiling and contact coiling in tendrils are active movements, that is, they require metabolic energy. However, tendrils also deform entirely passively based on water uptake or expulsion, a finding that renders them particularly interesting for the transfer of their movement into bioinspired technical materials systems. We observed passive movement for example when a young, yet unattached tendril was killed-off by immersion in a fixative such as ethanol. Despite the fixation in ethanol, the tendril started to curve when subsequently transferred to deionized water (Figure 1E, details can be found in Supporting Information). Moreover, fully coiled tendrils of several species have been shown to change in morphology with dehydration and rehydration,[8,19] which further illustrates the capability of passive motion. Triggered by the tendril's capability to move passively, we produced a variant of our artificial tendrils that coils upon the release of external stress, that is, "passively".

Four different MMF concepts have been employed in order to implement the various functions provided by the SMCF (Figure 2). A silicon-based soft elastomer was chosen as a matrix, whereas a cross-linked poly[ethylene-*co*-(vinyl acetate)] (cPEVA) fiber was selected as a core material for the synthesis of multimaterial fibers.[20]

In MMF-1, the SMCF can shrink upon heat thereby mimicking the shortening by developing G-fibers in tendrils. Here, the SMCF is programed into an elongated temporary shape before incorporation into the silicon matrix. The strain displacement in this case results from a shorter SMCF compared with the elastic silicon matrix (Figure 2B). The strain recovery of the core triggered by heat leads to the coiling of the MMF-1. The pre-strain magnitude has been reported to determine the curvature of the tendril predominantly in a proportional relationship.[12c] Therefore, the MMF-1 was fabricated from a deformed core (100%) and a non-annealed core, implying a moderate (≈35%) pre-straining from the extrusion process.

Coiling caused by passive deformation attributable water uptake is comparable to movement in MMF-2, in which the SMCF is incorporated into its permanent short length. A stretching deformation of MMF-2 after preparation leads to a programing of SMCF to a temporary long shape. In the functionalized MMF-2, the tough core fiber is longer than the elastic matrix (Figure 2C). Therefore, a coiled conformation is observed upon the release of external stress applied during the programing of SMCF. MMF-2 can uncoil on demand as heating triggers the recovery of the original length of the SMCF.

The concept of MMF-3 goes far beyond the blueprint from nature. Here, the crystallization and melting of domains from the oriented polymer chains in the SMCF fibers leads to a thermally controlled actuator. The reversible shape-memory effect is implemented in the SMCF by combining elongation and twisting (Figure 2D). The resulting macroscopic motion of the MMF-3 is determined and quantified. The number of twists were limited here to 30 twists per 10 cm to avoid any superstructures in the twisted fibers. The programed SMCF was firmly fixed and glued to the silicon matrix on the outside and did not move freely. The covalent cross-linking of SMCF allowed the deformation of these fibers by stretching and twisting before they were embedded in silicon. For the uncoiling MMF-2s, on the other hand, the covalent cross-linking of the core fiber might not be necessary. Here, the silicon shell possibly acts as a template and allows both deformation and the molecular orientation of the melted polymer core.

Finally, the arrangement of mechanical and actuating tissues in the cross sections of *B. alba* and *C. brachystachya* tendrils shown in Figure 1D has motivated the production of MMF-4, which contains a core with a U-shaped cross section. The MMF-4s behave similarly to MMF-1 (when containing a stretched U-shaped core) showing instant coiling on heating (Figure 2E) or coiling after a post-fabricating programing similar to that for MMF-2 (when containing a relaxed U-shaped core). The MMF-4 with the relaxed core also uncoils on heating similarly to MMF-2.

Microscopic images of cross sections of representative MMFs prepared according to the schematic representation in **Figure 2**A are shown in **Figure 3**B and reveal a bilayer structure with an overall thickness of ≈1 mm with a core (thickness ≈0.4 mm) embedded in the silicon matrix. An eccentric positioning of the SMCF is mostly observed in the silicon matrix, irrespective of the type of the MMF or of the fixation preferences (to achieve specific positioning) of the core prior to matrix curing. This is evident from the preliminary investigation of all round core MMFs as shown in Figure S3 (Supporting Information) followed by in depth evaluation for MMF-3 as can be seen in Figure S4 (Supporting Information). The positioning of the core was beyond control because of process constraints and the fact that, during silicon curing at ≈50 or 60 °C, the thermal expansion or contraction of the relaxed or pre-deformed SMCF might influence its own positioning. The position of the core was characterized by the distance between the center of gravity of the SMCF and the center of gravity of the MMF, as shown in Figure 3D,E, and by the angle of inclination of the straight line intersecting two centers. The results reveal the eccentric positioning of the core fiber, the position of which moves gradually along the length of the MMF. In rare cases, the position of the SMCF did not change along the length of the MMF, as can be seen in Figure S5 (Supporting Information). However, no significant difference in coiling behavior was observed.

The mismatch in modulus (by a factor of 8–20) and strain (≥30% and 0%) between core and shell, respectively, were the key parameters for the production of various MMFs. Therefore, the mechanical properties of the two components were studied and are discussed here in detail. The elastic modulus (E) of the silicon matrix was analyzed from the stress–strain experiments performed for cross-linked silicon fibers with an average diameter of ≈1 mm and revealed $E = 1.65 \pm 0.15$ MPa with a slight

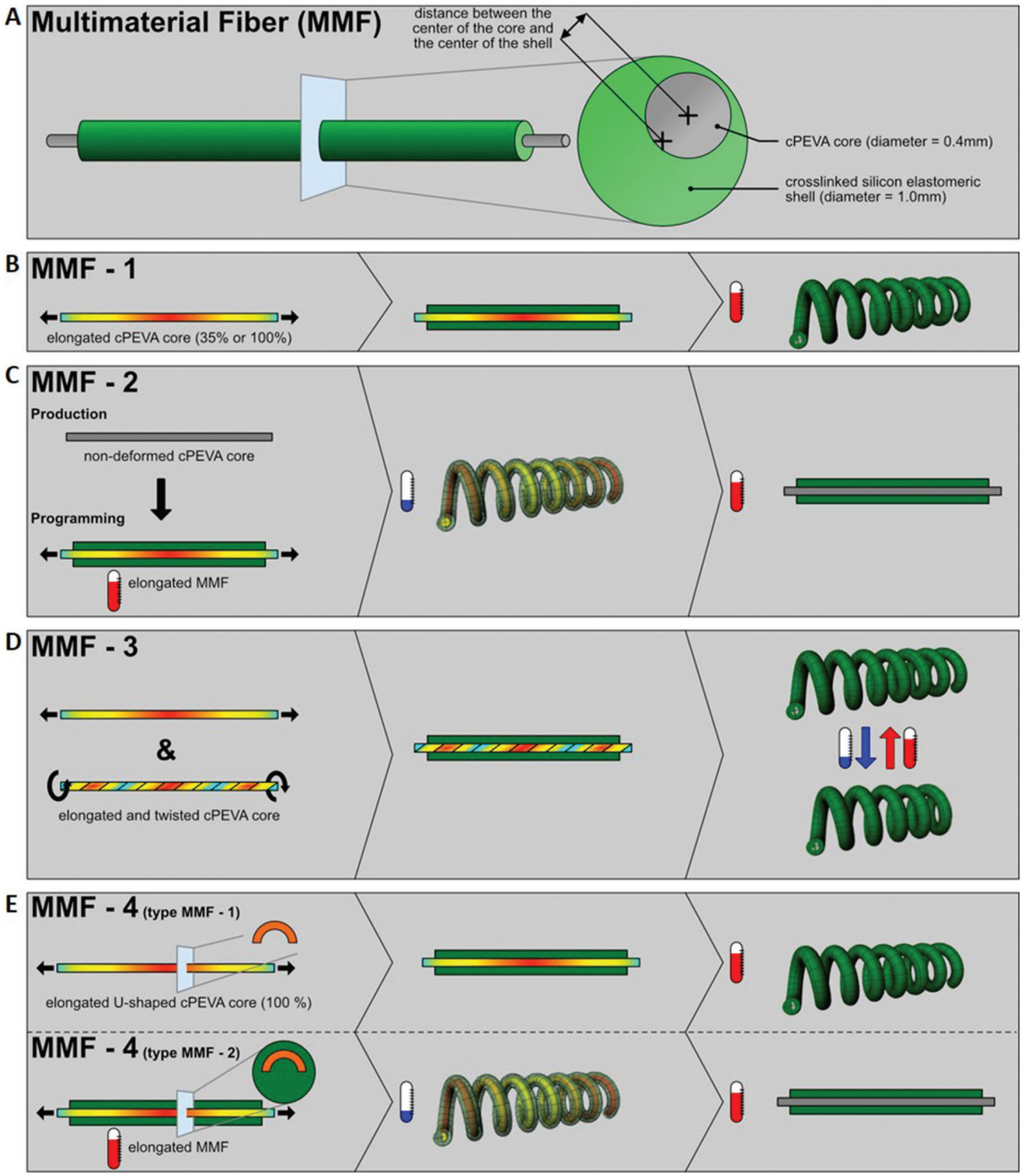

Figure 2. A) Schematic illustration of multimaterial fibers with a shape-memory fiber core and cross-linked silicon elastomer shell as a matrix. B) MMF-1 prepared from pre-strained/elongated SMCF (MMF-$1_{SMCF\text{-}100\%}$ or MMF-$1_{SMCF\text{-}35\%}$) that coil on heating. C) MMF-2 prepared from permanently shaped non-deformed SMCF, which does not change shape on heating. This MMF from permanently shaped SMCF can be programed by stretching at ≥65 °C followed by releasing stress at room temperature, leading to a coiled MMF that uncoils on heating (MMF-2). D) MMF-3 prepared from a deformed core (by stretching and twisting). These show a reversible change in the number of coils (MMF-3), coil diameter, and tendril length on cyclic heating and cooling. E) MMF-4 prepared from a U-shaped pre-strained or relaxed core that coils on heating similarly to MMF-1 or that coils on programing and uncoils on heating similarly to MMF-2.

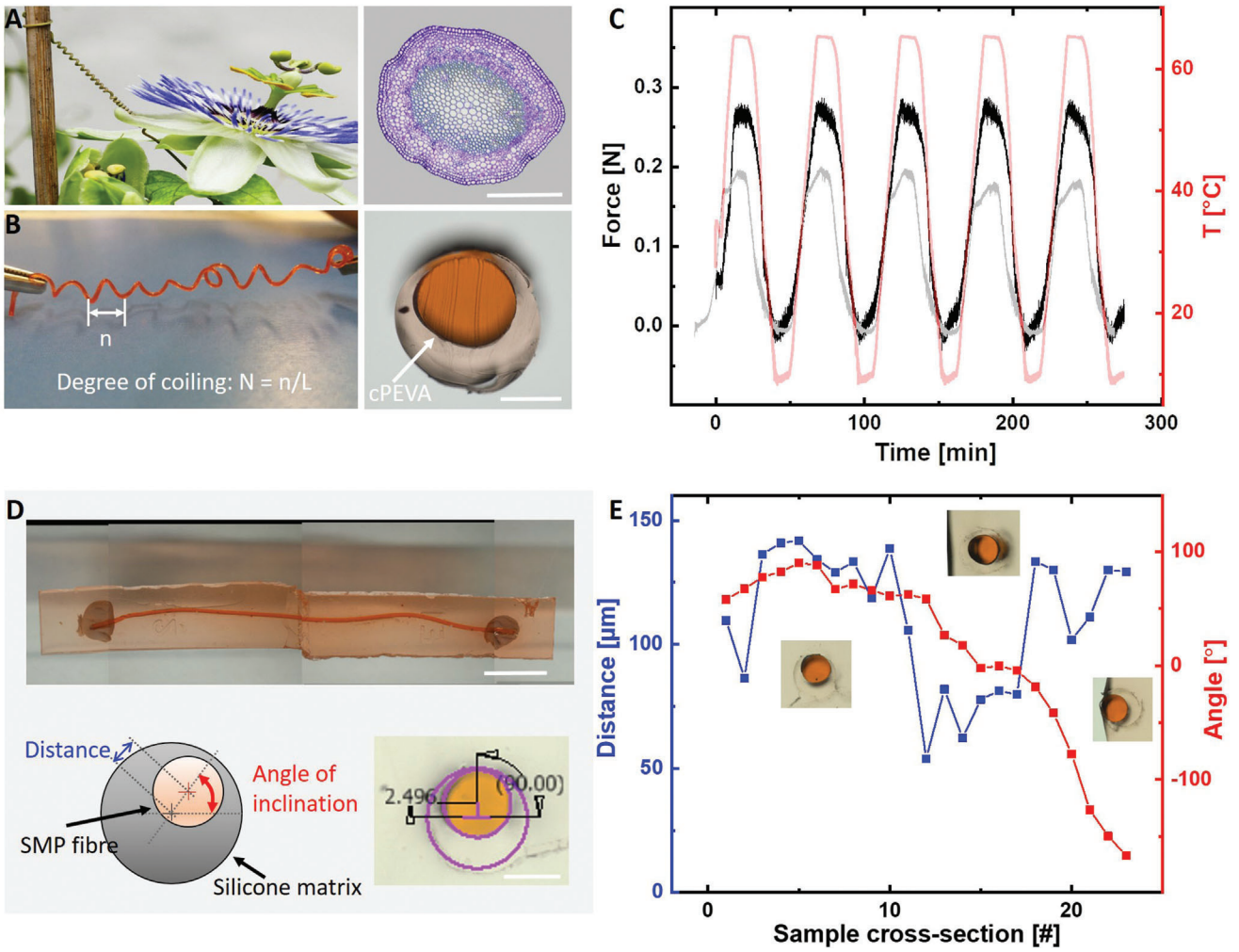

Figure 3. A) *P. caerulea* tendril attaching a plant stem with flower to a support, and toluidine-blue-stained cross section of a coiled tendril (scale bar: 400 µm). B) Coiled MMF with an image of its cross section (scale bar: 400 µm). C) Cyclic investigation of the recovery force of MMF-$1_{SMCF\text{-}100\%}$ (black) and MMF-$1_{SMCF\text{-}35\%}$ (gray) by respective heating and cooling between 10 and 65 °C (red) in a strain-controlled experiment. D) Cross-sectional analysis of the MMF with a shape-memory fiber core and cross-linked silicon elastomer shell as a matrix (scale bar: MMF in matrix—1 cm and cross-sectional image—200 µm). E) Resulting changes in the distance between the center of gravity of the core fiber and the center of gravity of the MMF (blue) and the angle of inclination along the length of MMF (red). See Figures S3–S5 (Supporting Information) for more cross-sectional images showing the position of the core.

difference in E being observed at ambient and elevated temperatures (65 °C). The resulting E of cross-linked silicon was suitable for a shell/matrix material for MMFs. The MMF-1 was fabricated with various levels of pre-straining as explained in Experimental section. The non-annealed core material was examined with respect to its extrusion-induced strain, which was ≈35% as determined from the shrinkage analysis, to produce MMF-1 with a 35% pre-strained core (MMF-$1_{SMCF\text{-}35\%}$). Additionally, the permanently shaped core material (after annealing) was further stretched to 100% in order to achieve higher pre-straining in MMF-$1_{SMCF\text{-}100\%}$. The E for the core was generally higher (between 12 and 33 MPa), a finding that was also dependent on the pretreatment of the core material. Annealing the core above the melting transition (≈80 °C) resulted in a lower $E = 12 \pm 3$ MPa when compared with the stretched core at ambient temperature with $E = 30 \pm 2$ MPa. A similar trend in E was observed at 65 °C (for details see **Table 1**). This difference in the modulus was attributable to the difference in the macromolecular orientation in the core related to the pretreatment. The difference in the modulus of both components made them good candidates for the production of MMFs. In all the studied MMFs, we observed that the silicon matrix broke around 80% strain at ambient temperature and at 65 °C. As expected, the elastic modulus of the MMFs was found to be higher than that of the matrix material and lower than that of the core material. At ambient temperature, the MMF-$1_{SMCF\text{-}100\%}$ showed the highest modulus $E = 11 \pm 2$ MPa with an elongation at break (ϵ_b) of ≈220 ± 40%, whereas a lower $E = 4.7 \pm 0.3$ MPa and $\epsilon_b = 120 \pm 25\%$ were observed at 65 °C. The lower values of E for the MMF-$1_{SMCF\text{-}35\%}$ and MMF-2 are related to the lower macromolecular orientation (see Table 1). The tensile results imply that an increase in the pre-strain of the core results in MMFs exhibiting a higher modulus with a much larger

Table 1. Mechanical properties of multimaterial fibers.

Composition	E [a] [MPa]	ϵ_b [b] [%]	E [c] [MPa]	ϵ_b [d] [%]	d [mm]
MMFs					
MMF-$1_{SMCF-100\%}$	11 ± 2	220 ± 40	4.7 ± 0.3	120 ± 25	0.9 ± 0.1
MMF-$1_{SMCF-35\%}$	6 ± 1.5	315 ± 50	3.5 ± 0.4	160 ± 50	0.85 ± 0.15
MMF-2	3 ± 0.5	515 ± 45	1.7 ± 0.2	300 ± 60	0.9 ± 0.1
Core material					
SMCF-100% [e]	30 ± 2	130 ± 5	11 ± 2	190 ± 30	0.38 ± 0.1
SMCF-35% [f]	33 ± 2	405 ± 40	-	-	0.4 ± 0.1
SMCF [g]	12 ± 3	590 ± 10	2 ± 0.15	255 ± 20	0.57 ± 0.3
Cross-linked matrix					
	1.8 ± 0.4	210 ± 20	1.5 ± 0.2	170 ± 15	0.9 ± 0.1

[a] E: Young's modulus determined by tensile tests at room temperature; [b] ϵ_b: Elongation at break at room temperature; [c] E: Young's modulus determined by tensile tests at 65 °C; [d] ϵ_b: Elongation at break at 65 °C; [e] *SMCF-100%*: Shape-memory core fiber in elongated temporary shape with 100% straining during programing; [f] *SMCF-35%*: Shape-memory core fiber in elongated temporary shape with extrusion induced strain of 35%; [g] *SMCF*: Shape-memory core fiber in permanent shape after annealing to remove extrusion induced orientation.

difference in the modulus between the matrix and core materials. These differences in pre-strain and modulus were further studied in terms of differences in the coiling behavior of the various MMFs.

2.1. MMF-1

The recovery force (F_r) was investigated for MMFs with pre-strained SMCF to investigate the stress stored in these MMFs. The F_r can be recorded over a range of temperatures, which is suitable to trigger the recovery of the core material from its pre-strained form. The MMFs are heated to 65 °C with a fixed strain, so that the coiling of the MMF can be avoided. The MMF with a 100% pre-strained core (MMF-$1_{SMCF-100\%}$) revealed a $F_r \approx 0.28$ N at 65 °C, as can be seen in Figure 3C, whereas a lower $F_r \approx 0.2$ N was observed for MMF-1 with 35% pre-straining (MMF-$1_{SMCF-35\%}$) resulting from the extrusion process. The F_r of MMFs was comparable with that of the core material, that is, we observed no changes in F_r after embedment in the silicon matrix and no influence of the matrix material on the recovery force of the core.

An MMF-1 (with SMCF in elongated temporary shape) tends to coil instantly as soon as it is exposed to an external stimulus, which in this case is heat. Heat triggers melt-induced contraction of the oriented polyethylene crystals within the broad melting transition temperature (T_m) of the SMCF.[21] Therefore, coiling is attributable to the entropy-elastic recovery of the core and the resulting strain mismatch between the core and elastic outer matrix; the MMF-1 turns into a coiled spring-like configuration as shown in Figure 3B and Video S2 (Supporting Information). This coiling behavior in MMFs is similar to the biological coiling principle found in tendrils with contractile fibers. The coiling curvature is related to the pre-straining degree: coils with a smaller diameter of $d \approx 0.4$ cm have been observed for MMF-$1_{SMCF-100\%}$ with high pre-straining and can be attributed to the related high F_r. The MMF-$1_{SMCF-35\%}$ also exhibited a coiled structure on heating: the larger coil diameter $d \approx 0.7$ cm was related to the lower degree of straining and the smaller F_r observed for these MMFs. A similar proportional relationship in the coil diameter and pre-straining was observed in bilayer type conductive tendrils,[12c] where pre-strains were varied from 30% to 400% and d decreased from 0.52 to 0.23 cm with increase in pre-strain. In the bilayer polymer–paper system, we found that the thickness of the polymer layer and the orientation of the printed polymer filaments on the paper substrate significantly affected the final bending deformation.[14] Polymer strips with a gradually varied thickness generated tendril-like spiral deformation, whereas various spatial arrangements of the printed filaments generated helical deformations.

In addition to the coil diameter, we calculated the degree of coiling (N), which is the number of coils per unit centimeter (from the length uncoiled MMFs). As expected from the values found for F_r and d, a larger $N = 0.60 \pm 0.08$ was observed for MMF-$1_{SMCF-100\%}$ compared with $N = 0.37 \pm 0.05$ for MMF-$1_{SMCF-35\%}$. Considerable variation in the degree of coiling (expressed as the ratio of straightened tendril length to coiled length) also occurs in biological tendrils.[22] Because the degree of coiling depends on the pre-straining and the resulting recovery forces in artificial tendrils, we can speculate that the biological variations might result from the different degrees of contraction attributable to variations in tissue development. Furthermore, the degree of coiling observed in plant tendrils might be influenced by the fact that, unlike in the experimental setup, the tendril is put under tension by the plant's weight (the shoot is dragged upward by the tendril, cf. Figure 1B). The degree of coiling actually achieved in the biological tendrils might thus also depend on the portion of the plant weight loaded on a particular tendril. The recovery from the coiled to an uncoiled shape has not been observed in MMF-1. For MMF-1, straining at ≥65 °C was required to adopt the initial uncoiled MMF form; this however might be exploited to achieve coiling. The incorporation of shape-memory materials in such a core–shell system allowed the MMFs having an on demand actuation as in MMF-1.

2.2. MMF-2

The F_r was also analyzed for the MMFs with relaxed/annealed/permanently shaped SMCF (MMF-2). However, no change occurred in the force with increase in temperature. In contrast, a small expansion on heating was determined in MMF-2 during the measurement. The recorded force was negative, and the experiments with a fixed strain did not allow this expansion to be detected. Because of the lack of F_r (or a small undetectable F_r), no coiling was observed in the MMF-2 upon initial heating. The coiling mechanism for these MMF-2s is different from those of MMF-1. Similar to the MMF-1, a strain mismatch/difference was required to achieve coiling, which was achieved by deformation or straining the MMF-2 after synthesis. The required straining was attained by stretching MMF-2 at 65 °C and subsequent quenching in cold water followed by release of the external stress. The MMF-2 coiled as soon as the external stress was released (see Video S3, Supporting Information). In a strained MMF-2, the (shape-memory) core tended to remain in its deformed shape, although the elastomeric coating shell tended to return back to its original length. Therefore,

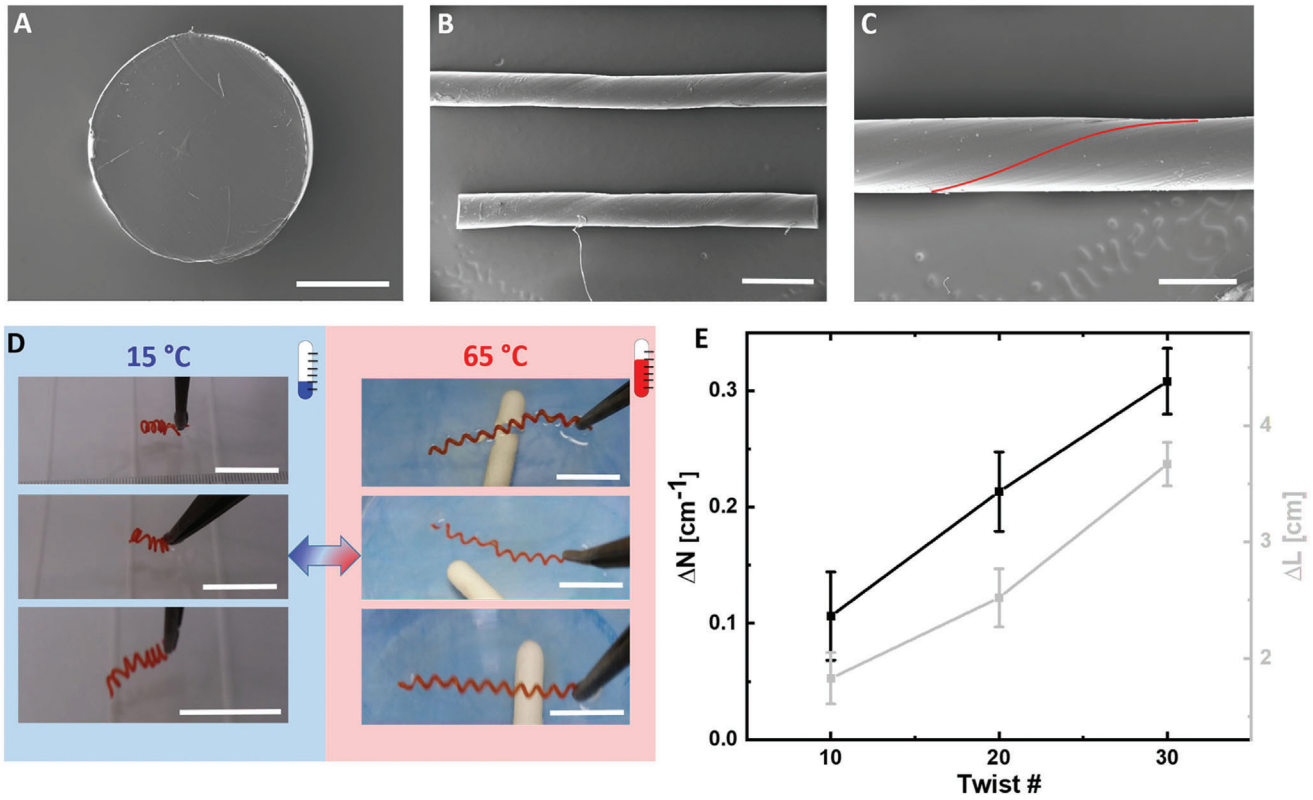

Figure 4. A–C) SEM images of a cross section of the twisted fiber (scale bar: 200 µm) (A) and the surface without (scale bar: 1 mm) and with a red guide line highlighting the spiral surface structure in the twisted fiber (scale bar: 500 µm) (B,C). D) Image series showing reversible opening and closing of three different MMF-3 tendrils on heating and cooling, during the 3rd heating–cooling cycle (scale bar 2 cm). E) Effect of number of twists on the reversible change in length (ΔL) and degree of coiling (ΔN). Data of five samples (mean ± standard deviation) for each number of twists measured within the 3rd cycle of each sample.

as soon as the external stress on the MMF-2 was released, it turned into a coiled conformation. A high degree of coiling $N = 0.5 \pm 0.07$ was observed for these MMFs when they were stretched to a defined strain of 50%. A change in the straining magnitude during deformation led to different N. Almost no coiling was observed with strains ≤30%, that is, strains of >30% were required to obtain coiling in these MMFs. The increase in N with increase in strain can clearly be seen in Figure S6B (Supporting Information), where a maximum $N = 0.57 \pm 0.8$ is observed for the highest applied strain of ≈60%. Further straining led to the break of the silicon matrix and delamination. Therefore, the MMF-2 could not be strained >60% to achieve more intense coiling. The delamination might be attributed to the weak bonding between the pre-cross-linked SMCF and the thin silicon matrix layer. The change in the coiling degree is shown in the image series presented in Figure S6A (Supporting Information) for various strains. Each sample was reprogramed 3–5 times at specific strain and the images were taken after at least three programing cycles at certain strain. It can be seen from the presented images that no delamination occurs if the MMFs were programed ≤60% strain and prove the durability of the MMFs for extended number of cycles. Uncoiling of MMF-2 samples can be observed by heating to 65 °C as demonstrated in Video S3 (Supporting Information). The uncoiling mechanism is related to the recovery of the core with change in temperature. The straining required to achieve coiling in MMF-2 can be repeated as long as the silicon matrix is not damaged in the programing. The repeatability of this programing is shown in Figure S6A (Supporting Information), where an individual MMF-2 is deformed multiple times to different strain degrees to achieve different N. The design of MMF-2 gives the opportunity to induce coiling in post fabrication step, which can also be erased and process can be repeated to achieve a different degree of coiling by simply varying the strain applied in programing. This has not been reported in other bilayer coiling systems.

2.3. MMF-3

MMF-3 samples prepared by a core deformed by stretching and twisting exhibited coiling immediately when they were heated (see Figure 2D). The microscopic images of the deformed core fiber revealed a spiral surface structure confirming twisting in the fiber (see **Figure 4**B,C). The cross section of the core however did not show any changes after deformation by stretching and twisting (Figure 4A). The degree of coiling ($N = 0.7 \pm 0.05$) and the coil diameter ($d \approx 0.43$ cm) was similar to those for MMF-$1_{\text{SMCF-100\%}}$, which contained a stretched core with 100% strain without twisting. The similarity in this behavior can be attributed to the same stretching deformation (100%) of these two types

of MMFs. Nevertheless, the coiled structure of MMF-3 takes up a compressed-spring-like configuration when cooled down, as can be seen in Figure 4D. Similar contractive smart spring-like movements have been shown for hierarchically arranged helical fibers (HHFs) that respond to solvent and vapor.[12a] These HHFs are created through the hierarchical and helical assembly of aligned carbon nanotubes. However, they either show contraction or elongation (based on their chirality) in response to solvent exposure, whereas in our system, the movement is reversible with contraction upon cooling and elongation upon heating as can be observed in Video S4 (Supporting Information). The reversible actuation process can be repeated several times, and a similar reversible change in length can be obtained in subsequent cycles. The core deformation in these tendrils was varied by changing the number of twists to 10, 20, and 30 twists per 10 cm length, whereas the initial deformation by stretching was a constant 100%. The results for different amounts of twisting were analyzed and compared (see Figure 4E). The N and d were in a similar range for these MMF-3 samples with different degrees of twisted core material. However, an increase in the reversible change in length (ΔL) was observed with increasing number of twists. Here, a change from 1.5 to 4 cm in ΔL was observed with a change in number of twists from 10 to 30. A high actuation magnitude of up to ≈400% was observed in these reversibly actuating MMFs, which is at least 20-fold higher compared with soft actuators based on shape-memory polymers, which mostly have a smaller reversible actuation ≤20%. This reversible length change also results in a change of the degree of coiling (ΔN). The ΔN was calculated by the difference of N at 65 °C and N at 15 °C. The number of coils increased on heating and decreased reversibly on cooling during the reversible actuation in MMF-3. The ΔN changed from ≈0.1 to ≈0.3 with a change in number of twists from 10 to 30. The observed reversible actuation is a result of the combined effect of stretching and twisting. Cross-sectional analyses of coiled MMFs showed a similar positioning of the core fiber, where the core fiber was either located on the outer side of the macroscopic spiral or, in some sections, on the inner side.

The reversible effect is a combined effect of this core–shell fiber multimaterial system, in which the core fibers must firmly adhere to the silicon matrix to avoid an independent actuation of the core material, namely a linear contraction and expansion or reversible twisting and untwisting. In SMP-based actuators, heating to a transition temperature T_{high} leads to the melting of some crystallites and consequently a partial recovery from a temporary shape (to another temporary shape), a finding that is true for linear and torsional fiber actuators as observed by partial contraction or untwisting upon heating, respectively. The recrystallization upon cooling leads to a reciprocal response such as elongation or twisting in the programing/deformation direction. In these actuating MMF-3, this implies a contraction/compression and untwisting on heating and vice versa. However, the embedding of pre-twisted and pre-strained SMCF in silicon has somehow reversed the effect, whereby an expansion and an increase in the number of coils is observed on heating and vice versa. These multimaterial fibers can be actuated as long as the core and shell adhere to each other and are not delaminated. The MMF-3 allows a unique reversible coiling actuation that has not been reported in any soft actuating system before, where in addition to the innovative spring like reversible coiling movements, the actuation magnitude exceeds the performance of comparable soft actuator systems.

2.4. MMF-4

MMF-4 was prepared from the U-shape core for which PEVA tubes were extruded and sliced as described in the Experimental section. Such MMFs with a stretched core showed instant coiling upon heating, similarly to MMF-1; however, the degree of coiling $N = 0.4 \pm 0.1$ was lower, as can been seen Figure S7 (Supporting Information). The MMF with non-deformed U-shape core behaved similarly to MMF-2, for which coiling can be achieved in a post-synthesis programing procedure and uncoiling on heating. Here again, the degree of coiling was lower when compared with MMF-2. Because of the smaller N, these MMFs were not further considered for further in-depth evaluation. The smaller N in U-shape MMFs might be attributed to the lower entropic recovery force of such a core due to different orientation of molecular chains and crystallites, which are dispersed over the U-shape and the core itself is filled with silicon in the center in contrast to a compact round SMCF. Furthermore, the pre-strained and pre-twisted core-based MMFs were not possible with this approach (which are more suitable as reversible actuating MMFs, similar to MMF-3) because of the limitations of U-shape core for only linear deformation. Therefore, the work on U-shape core MMFs was considered out of the scope of this study.

Typical fiber actuators have two actuation modes, linear contraction and expansion or reversible twisting and untwisting. Here, we have reported reversible coiling movements in such MMFs that can be envisioned as fiber actuators, such as artificial muscles in future soft robotic applications. Furthermore, these MMFs are envisioned as actuating and support elements for plant inspired growing robots similar to the tendrils in natural plants; however, a validation of these MMFs in comparison to the natural tendrils is required. With this new actuation mode, these fibers allow a much larger actuation magnitude when compared to conventional soft actuators. Although these MMFs have limitations due to their smaller force, the fabrication principles disclosed in this work can be extended to other materials to create similar MMFs but with enhanced properties.

3. Conclusion

We have abstracted the design principles from plant tendrils as the starting point for creating MMF with a SMCF. We do not claim to have made a full artificial "copy" of the natural tendrils, which show complex metabolic processes involved in coiling. In our opinion, this would be neither feasible nor desirable and does not represent a promising way to do biomimetics research. Abstraction and meaningful simplifications are inherent processes in any successful biomimetic transfer process as done in the present study. From several principles involved in coiling movement in plant tendrils, we identified the strain mismatch brought about by contractile fibers present in tendrils of many species of climbing plants as being the most suitable one for transfer into an artificial tendril and illustrated its functioning as a basis for developing an MMF. The strain mismatch, eccentric positioning of

the core, and relevant molecular orientation in the core were considered the key parameters to achieve coiling. The modulus of the core materials was between 12 and 35 MPa depending on their pretreatment that decreases with increase in temperature (during consequent recovery movement). These fibers were imbedded in a low modulus ≈1.6 MPa matrix material to achieve MMFs. The difference in the strain and the related recovery behavior of two materials was used as a control parameter to achieve various coiling behaviors in these MMFs. The microscopic images of the artificial tendril's cross sections revealed the eccentric positioning of the core in the silicon matrix. In MMF-1 tendrils, a high degree of coiling $N = 0.6 \pm 0.08$ was observed instantly on exposure to an external stimulus. The coiling was related to the recovery of the pre-strained core material upon heating to its recovery temperature ≈65 °C. A maximum recovery force of ≈0.3 N was observed for these tendrils. The MMF-2 tendrils with a relaxed core were deformed after synthesis to achieve similar coiling, which was undone upon heating. Finally, the reversibly actuating tendrils of the type MMF-3 showed a high magnitude of reversible actuation ≈400%, related to the actuation from the combined deformation of the core, such as by stretching and twisting, together with the elastomeric shell. These MMF-3 show artificial (soft) plant-like movements and can be envisioned as fiber actuators, such as artificial muscles, in future soft robotic applications.

4. Experimental Section

Materials: Climbing plant species *C. brachystachya*, *B. alba*, *P. caerulea*, and *P. discophora* were cultivated in the Botanical Garden of Freiburg University either out of doors or in the greenhouse. Two fixatives were used for the plant samples, either ≥99.8% ethanol (Carl Roth, Karlsruhe, Germany) or formaldehyde–acetic acid (FAA), namely a mixture of 70 vol% ethanol (Carl Roth, Karlsruhe, Germany), formol (37% formaldehyde solution, ROTIPURAN, Carl Roth, Karlsruhe, Germany), and glacial acetic acid (Carl Roth, Karlsruhe, Germany) (90:5:5 v/v/v). A series of increasing isopropanol (Carl Roth, Karlsruhe, Germany) concentrations was used for dehydration. Samples were embedded in plastic (Technovit 7100, Kulzer, Hanau, Germany), and thin sections were stained with toluidine blue solution (0.05 wt% , toluidine blue O, Sigma Chemical, St Louis, MO, USA).

For the multimaterial fibers (MMFs), a silicon elastomer base and curing agent (SYLGARD 184 Silicone Elastomer Kit) (Dow chemicals, Midland, Michigan, USA) were used as delivered by the manufacturer. Polytetrafluoroethylene (PTFE) tubes with an inner diameter of 1, 1.5, or 2 mm (VWR International GmbH, Radnor, PA, USA) were employed to prepare molds. Cross-linked poly[ethylene-*co*-(vinyl acetate)] (cPEVA) fibers were used as core material.[20]

Methods: *Extrusion*: PEVA tubes were extruded from the blend granulates (PEVA 99 wt% and TAIC 1 wt%) using tubular dies with an outer diameter of 0.8 mm and inner diameter of 0.6 mm in a single screw extruder (Extrudex, Mühlacker, Germany). The diameter of the tubes was further adjusted by controlling the winding speed and the speed of the screw. Poly[ethylene-*co*-(vinyl acetate)] (PEVA) with a vinyl acetate content of 28 wt% (Elvax 260A, DuPont, DE, USA) and triallyl isocyanurate (TAIC) (99%, Sigma–Aldrich, Steinheim, Germany) were used as delivered by the manufacturer for tube synthesis. After fabrication by extrusion, the tubes were cross-linked by a gamma beam of 165 kGy in a post-synthesis process. The cross-linked tubes were cut in half to make U-shape core material, which was used to fabricate MMFs.

Fabrication of Multimaterial Fibers (MMFs): Silicon elastomer base and curing agent were mixed in a 13:1 ratio with 0.2 wt% dye and degassed under vacuum for 30 min to remove air bubbles. Molds were prepared by cutting PTFE tubes on a hotplate at 150 °C and straightening them. The inner molding tube was cut through the middle from one end, to ≈5 mm from the other end, such that the two halves were still attached to each other (see Figure S2A, Supporting Information). A second tube with the larger diameter served as a casing for the inner mold to avoid the flow of the solution out of the mold. The outer casing tube was cut on one side along its length for easier insertion and removal of the inner mold. Core material is then inserted into the inner molding tube (Figure S2B, Supporting Information). The position of the core in the mold was adjusted in the middle or toward one side of the mold by fixing the core in the center by clamps or by fixing it by folding/sliding it into the outer casing. The mold was then closed on one side by using Teflon tape, while the other side was left open until the insertion of the solution (Figure S2C, Supporting Information). Filled molds were finally inserted into a glass reactor and were placed in water bath at 50 or 60 °C overnight for curing (Figure S2D,E, Supporting Information). This synthesis was employed for all investigated multimaterial fibers. The exact eccentricity of the SMCFs in the MMFs could not be controlled with high accuracy because of the chosen production procedure, namely the coiling of the MMFs was caused by an eccentric positioning of the core.

MMF-1: Embedded SMCF in Pre-Strained Temporary Shape: The core was programed by stretching it before its insertion into the molds. At first, it was relaxed at 80 °C. The relaxed core was then programed by stretching to 100% at 80 °C followed by quenching in ice-cold water ≈5 °C to prepare multimaterial fibers (Figure 2B). In addition, non-annealed (non-relaxed) core material with 35% strain from extrusion process was used to prepare multimaterial fibers for comparison. These MMFs with a programed core were designated as MMF-$1_{\text{SMCF-35\%}}$ and MMF-$1_{\text{SMCF-100\%}}$ respective to the strain in SMCF.

MMF-2: Embedded SMCF in Permanent Shape: These multimaterial fibers were achieved by using a relaxed core. The relaxation of extrusion-induced strains/stresses was achieved by heating in a water bath at 80 °C followed by cooling. These relaxed core materials were inserted into the molds and fixed (Figure 2C).

MMF-3: SMCF in Temporary Shape Obtained by Stretching and Twisting: At first, the core materials were relaxed. Then, they were deformed by stretching to 100% followed by a second deformation step by twisting. The number of twists varied: 10, 20, and 30 twists per 10 cm core material length (Figure 2D).

MMF-4: Shape-Memory Core with U-Shaped Cross Section: Cores with a U-shaped cross section were obtained by slicing cPEVA tubes in the middle and were imbedded in silicon matrix in a deformed/elongated temporary shape with a strain ≈100% (during programing) similar to that of MMF-1 or in permanent shape as in MMF-2. The obtained MMFs with cores having a U-shaped cross section were analyzed for their coiling and uncoiling behavior, as were MMFs with cores having a circular cross section. Further details on the methodology can be found in Supporting Information.

Supporting Information

Supporting Information is available from the Wiley Online Library or from the author.

Acknowledgements

M.F. and F.K. contributed equally to this work. The authors thank Florian Kröber, Yvonne Pieper, and Michael Schmidt for technical support and Dr. Axel Neffe for his support in manuscript preparation. This work was financially supported by the Helmholtz Association through program-oriented funding and received funding from the European Union's Horizon 2020 research and innovation program under Grant Agreement No. 824074 (GrowBot). T.S. and F.K. acknowledge additional funding by the DFG (Deutsche Forschungsgemeinschaft) under Germany's Excellence Strategy, EXC-2193/1-390951807.

Open access funding enabled and organized by Projekt DEAL.

Conflict of Interest

The authors declare no conflict of interest.

Data Availability Statement

The data that support the findings of this study are available from the corresponding author upon reasonable request.

Keywords

actuators, elastic modulus, multimaterial fibers, pre-straining, tendrils

Received: December 19, 2022
Revised: March 20, 2023
Published online:

[1] a) R. Sachse, A. Westermeier, M. Mylo, J. Nadasdi, M. Bischoff, T. Speck, S. Poppinga, *Proc. Natl. Acad. Sci. USA* **2020**, *117*, 16035; b) S. Armon, E. Efrati, R. Kupferman, E. Sharon, *Science* **2011**, *333*, 1726; c) R. Elbaum, L. Zaltzman, I. Burgert, P. Fratzl, *Science* **2007**, *316*, 884; d) J. Gallentine, M. B. Wooten, M. Thielen, I. D. Walker, T. Speck, K. Niklas, *Front. Rob. AI* **2020**, *7*, 118.

[2] a) S. Isnard, W. K. Silk, *Am. J. Bot.* **2009**, *96*, 1205; b) C. R. Darwin, *The Movements and Habits of Climbing Plants*, John Murray, London, UK **1882**; c) N. P. Rowe, T. Speck, in *Ecology of Lianas* (Eds: S. A. Schnitzer, F. Bongers, R. J. Burnham, F. E. Putz), John Wiley & Sons, Ltd, New York **2015**, 323; d) K. C. Vaughn, A. J. Bowling, in *Horticultural Reviews* (Ed: J. Janick), Vol. *38*, John Wiley & Sons, Ltd, New York **2011**, p. 1.

[3] a) M. J. Jaffe, A. W. Galston, *Ann. Rev. Plant Physio.* **1968**, *19*, 417; b) D. T. MacDougal, *Ann. Bot.* **1896**, *10*, 373; c) D. T. MacDougal, *Bot. Gaz.* **1893**, *18*, 123.

[4] A. Goriely, M. Tabor, *Phys. Rev. Lett.* **1998**, *80*, 1564.

[5] a) T. McMillen, A. Goriely, *J. Nonlinear Sci.* **2002**, *12*, 241; b) P. Pieranski, J. Baranska, A. Skjeltorp, *Eur. J. Phys.* **2004**, *25*, 613.

[6] M. J. Jaffe, A. W. Galston, *Plant Physiol.* **1966**, *41*, 1014.

[7] A. J. Bowling, K. C. Vaughn, *Am. J. Bot.* **2009**, *96*, 719.

[8] S. J. Gerbode, J. R. Puzey, A. G. McCormick, L. Mahadevan, *Science* **2012**, *337*, 1087.

[9] a) T. Steinbrecher, E. Danninger, D. Harder, T. Speck, O. Kraft, R. Schwaiger, *Acta Biomater.* **2010**, *6*, 1497; b) F. Putz, N. Holbrook, in *The Biology of Vines* (Eds: F. E. Putz, H. A. Mooney), Cambridge University Press, Cambridge, UK **1991**, p. 73.

[10] B. Mazzolai, I. Walker, T. Speck, *Front. Rob. AI* **2021**, *8*, 711942.

[11] a) C. M. Flynn, J. R. Puzey, *Integr. Comp. Biol.* **2017**, *57*, E52; b) M. H. Godinho, J. P. Canejo, L. F. V. Pinto, J. P. Borges, P. I. C. Teixeira, *Soft Matter* **2009**, *5*, 2772; c) S. K. Wong, K. C. Chen, *Comput. Graph Forum* **2016**, *35*, 5.

[12] a) P. N. Chen, Y. F. Xu, S. S. He, X. M. Sun, S. W. Pan, J. Deng, D. Y. Chen, H. S. Peng, *Nat. Nanotechnol.* **2015**, *10*, 1077; b) Y. Y. Zhao, X. R. Miao, J. Y. Lin, X. H. Li, F. G. Bian, J. Wang, X. Z. Zhang, B. H. Yue, *Global Challenges* **2017**, *1*, 1600021; c) Y. Cheng, R. R. Wang, K. H. Chan, X. Lu, J. Sun, G. W. Ho, *ACS Nano* **2018**, *12*, 3898.

[13] a) S. Iamsaard, S. J. Asshoff, B. Matt, T. Kudernac, J. J. L. M. Cornelissen, S. P. Fletcher, N. Katsonis, *Nat. Chem.* **2014**, *6*, 229; b) L. T. de Haan, J. M. N. Verjans, D. J. Broer, C. W. M. Bastiaansen, A. P. H. J. Schenning, *J. Am. Chem. Soc.* **2014**, *136*, 10585; c) L. Hines, K. Petersen, G. Z. Lum, M. Sitti, *Adv. Mater.* **2017**, *29*, 1603483; d) A. Lendlein, *Sci. Rob.* **2018**, *3*, eaat9090.

[14] W. Wang, C. Li, M. Cho, S. H. Ahn, *ACS Appl. Mater. Interfaces* **2018**, *10*, 10419.

[15] J. M. Boothby, T. H. Ware, *Soft Matter* **2017**, *13*, 4349.

[16] a) Z. L. Wu, M. Moshe, J. Greener, H. Therien-Aubin, Z. H. Nie, E. Sharon, E. Kumacheva, *Nat. Commun.* **2013**, *4*, 1586; b) H. Therien-Aubin, Z. L. Wu, Z. H. Nie, E. Kumacheva, *J. Am. Chem. Soc.* **2013**, *135*, 4834.

[17] D. T. MacDougal, *Bot. Gaz.* **1892**, *17*, 205.

[18] A. F. Abouraddy, M. Bayindir, G. Benoit, S. D. Hart, K. Kuriki, N. Orf, O. Shapira, F. Sorin, B. Temelkuran, Y. Fink, *Nat. Mater.* **2007**, *6*, 336.

[19] J. S. Wang, G. Wang, X. Q. Feng, T. Kitamura, Y. L. Kang, S. W. Yu, Q. H. Qin, *Sci. Rep.* **2013**, *3*, 3102.

[20] M. Farhan, D. Chaudhary, U. Nochel, M. Behl, K. Kratz, A. Lendlein, *Macromol. Mater. Eng.* **2021**, *306*, 2000579.

[21] M. Farhan, M. Behl, K. Kratz, A. Lendlein, *MRS Commun.* **2021**, *11*, 476.

[22] F. Klimm, S. Schmier, H. F. Bohn, S. Kleiser, M. Thielen, T. Speck, *J. Exp. Bot.* **2021**, *73*, 1190.